The 2019 super-Eddington outburst of RX J0209.6−7427: Detection of pulsations and constraints on the magnetic field strength

G. Vasilopoulos ⓘ ,[1]⋆ P. S. Ray ⓘ ,[2] K. C. Gendreau,[3] P. A. Jenke,[4] G. K. Jaisawal ⓘ ,[5]
C. A. Wilson-Hodge ⓘ ,[6] T. E. Strohmayer ⓘ ,[7] D. Altamirano ⓘ ,[8] W. B. Iwakiri,[9]
M. T. Wolff ⓘ ,[2] S. Guillot ⓘ ,[10] C. Malacaria ⓘ ,[6,11]† A. L. Stevens[12,13]

[1]*Department of Astronomy, Yale University, PO Box 208101, New Haven, CT 06520-8101, USA*
[2]*Space Science Division, U.S. Naval Research Laboratory, Washington, DC 20375, USA*
[3]*X-Ray Astrophysics Laboratory, NASA Goddard Space Flight Center, Greenbelt, MD 20771, USA*
[4]*University of Alabama in Huntsville, Huntsville, AL 35805, USA*
[5]*National Space Institute, Technical University of Denmark, Elektrovej 327-328, DK-2800 Lyngby, Denmark*
[6]*Astrophysics Branch, NASA Marshall Space Flight Center, Huntsville, AL 35812, USA*
[7]*Astrophysics Science Division and Joint Space-Science Institute, NASA's Goddard Space Flight Center, Greenbelt, MD 20771, USA*
[8]*School of Physics and Astronomy, University of Southampton, Southampton, SO17 1BJ, UK*
[9]*Department of Physics, Faculty of Science and Engineering, Chuo University, 1-13-27 Kasuga, Bunkyo-ku, Tokyo 112-8551, Japan*
[10]*IRAP, CNRS, 9 avenue du Colonel Roche, BP 44346, F-31028 Toulouse Cedex 4, France*
[11]*Universities Space Research Association, NSSTC, 320 Sparkman Drive, Huntsville, AL 35805, USA*
[12]*Department of Physics & Astronomy, Michigan State University, 567 Wilson Road, East Lansing, MI 48824, USA*
[13]*Department of Astronomy, University of Michigan, 1085 South University Avenue, Ann Arbor, MI 48109, USA*

ABSTRACT

In November 2019, MAXI detected an X-ray outburst from the known Be X-ray binary system RX J0209.6−7427 located in the outer wing of the Small Magellanic Cloud. We followed the outburst of the system with *NICER* which led to the discovery of X-ray pulsations with a period of 9.3 s. We analyzed simultaneous X-ray data obtained with *NuSTAR* and *NICER* allowing us to characterize the spectrum and provide an accurate estimate of its bolometric luminosity. During the outburst the maximum broadband X-ray luminosity of the system reached $1–2\times10^{39}$ erg s^{-1}, thus exceeding by about one order of magnitude the Eddington limit for a typical 1.4 $M_\odot$ mass neutron star (NS). Monitoring observations with *Fermi*/GBM and *NICER* allowed us to study the spin evolution of the NS and compare it with standard accretion torque models. We found that the NS magnetic field should be of the order of 3×10^{12} G. We conclude that RX J0209.6−7427 exhibited one of the brightest outbursts observed from a Be X-ray binary pulsar in the Magellanic Clouds, reaching similar luminosity level to the 2016 outburst of SMC X-3. Despite the super-Eddington luminosity of RX J0209.6−7427, the NS appears to have only a moderate magnetic field strength.

Key words: X-rays: binaries – galaxies: individual: SMC – stars: neutron – pulsars: individual: RX J0209.6−7427

1 INTRODUCTION

High mass X-ray binaries (HMXBs) are young binary systems where the massive companion (typically $> 8M_\odot$) transfers material onto a compact object. A major subclass of HMXBs are Be X-ray binaries (BeXRBs), a population that hosts the majority of the known X-ray pulsars (Reig 2011, for a review on BeXRBs). Among BeXRBs the vast majority host a Neutron Star (NS) as

a compact object. At the moment MWC 656 is the only blackhole BeXRB known (Casares et al. 2014), while a couple candidate White Dwarf BeXRBs have been reported (e.g. Haberl 1995; Torrejón & Orr 2001; Sturm et al. 2012). In BeXRBs the donor is a Be star that loses material through a slow moving equatorial wind that is referred to as decretion disk. As the binary plane can be misaligned to the decretion disk or the NS orbit can be highly eccentric, mass transfer is not constant and thus BeXRBs are typically highly variable systems. X-ray outbursts are typically observed as the NS passes through the Be disk. Type I or normal outbursts have duration shorter than the orbital period and reach luminos-

---

⋆ E-mail: georgios.vasilopoulos@yale.edu
† NASA Postdoctoral Fellow

ity ~10% the Eddington limit for a NS ($L_{\rm Edd}$ = 2×10^{38} erg/s, assuming a NS mass of 1.4 $M_\odot$). Type II or giant outbursts are less frequent and can last several orbits while reaching luminosities in excess of $L_{\rm Edd}$ (see Okazaki & Negueruela 2001; Okazaki et al. 2013; Martin et al. 2014, for various outbursts mechanisms).

In X-ray pulsars, the strong magnetic field of the NS disrupts the flow of matter at a distance where the magnetic field pressure equals the ram pressure of the flow. Material is then funneled along the field lines onto the magnetic pole, forming the so-called accretion column (Basko & Sunyaev 1976). The emission characteristics of this region depend on the mass accretion rate, as for large values a shock develops above the NS surface. By following the evolution of X-ray outbursts in BeXRBs we can gain insight on the radiative processes in the accretion column and the formation of the shock above the NS surface that is believed to define the transition between subcritical and supercritical accretion regimes. For many systems, this transition has been observationally determined to occur close to X-ray luminosities of 10^{37} erg s^{-1} (see characteristic example of EXO 2030, Reig & Nespoli 2013; Epili et al. 2017), as below (above) this critical L_X the spectra of the systems become harder (softer) when brighter (typically within 2.0–10.0 keV band).

In addition, major outbursts of BeXRBs have historically offered the first evidence that accretion onto NSs can at least momentarily exceed $L_{\rm Edd}$. However, the discovery of pulsations from M82 X-2, a system with luminosity of $100 \times L_{\rm Edd}$, demonstrated that stable accretion onto NSs at super-Eddington rate is possible (Bachetti et al. 2014). This discovery introduced a new category of systems, the so-called pulsating ultra-luminous X-ray sources (PULXs), that are broadly defined as extragalactic accreting NSs with luminosities greater than 10^{39} erg s^{-1} (see Kaaret et al. 2017, for a review on ULXs). This realization has fueled a search that led to the discovery and study of more PULXs in recent years (e.g., Fürst et al. 2016; Israel et al. 2017; Carpano et al. 2018; Rodríguez Castillo et al. 2019; Sathyaprakash et al. 2019). Furthermore, based on spectral similarities between non-pulsating and pulsating ULXs, there is now compelling evidence that a significant fraction of ULXs may host highly magnetized NSs (Koliopanos et al. 2017; Pintore et al. 2017; Walton et al. 2018a). In the broad sense, the brightest giant outbursts from BeXRBs ($L_X > 10^{39}$ erg s^{-1}) temporarily qualify these systems as PULXs. However, there are a few key differences between the two categories of systems. Although both systems can show large variability in their X-ray flux (factor >100), in BeXRBs this is a result of variable mass transfer, while in extragalactic PULXs, mass transfer is stable through many orbits and variations in their observed flux occur in quasi-periodic super-orbital time scales, and are thought to be related to obscuration due to disk precession (Dauser et al. 2017; Fürst et al. 2017; Vasilopoulos et al. 2019; Middleton et al. 2019).

In order to explain the super-Eddington luminosities of PULXs, it has been speculated (Mushtukov et al. 2015) that the NSs in these systems must have high magnetic field strengths ($B > 10^{13}$ G), which is at least an order of magnitude larger than NSs in typical X-ray pulsars (Ho et al. 2014). Albeit, in the recent work of King & Lasota (2019), the authors claim that the observed properties of many PULXs can be explained by NS with magnetic field strength between 10^{11}–10^{13}G. A characteristic example is the PULX system NGC300 ULX1 where the NS magnetic field (dipole term of ~ 10^{12} G) has been constrained by both timing studies (Vasilopoulos et al. 2018b, 2019) and the possible detection (see caveats, Koliopanos et al. 2019) of a cyclotron line (Walton et al. 2018b). However, there are at least a couple of systems that their temporal properties probe magnetic fields similar to magnetar values (e.g., M81 X-2 and M51 ULX-7, Bachetti et al. 2020; Vasilopoulos et al. 2020). Nevertheless, the radiative mechanisms of the NS accretion column (Becker & Wolff 2007) have not yet been fully studied at super-Eddington accretion rates, where several assumptions break due to the accretion column geometry (West et al. 2017).

Given that the handful of persistent PULXs that are known lie at distances of a few Mpc, their detailed study is hampered by limitations of current X-ray observatories. While this might change with the launch of future proposed missions (e.g., STROBE-X and eXTP, Ray et al. 2019; Zhang et al. 2019), at the moment the best laboratories to study super-Eddington accretion are major outbursts of BeXRBs in our local galaxy group. Perhaps the brightest X-ray outburst of a BeXRB was the 2017 outburst of the Galactic pulsar Swift J0243.6+6124 making it the first Galactic PULX (luminosity of ~2×10^{39} erg s^{-1}; Wilson-Hodge et al. 2018). However, an ideal place to study BeXRBs are the nearby star-forming Magellanic Clouds (MCs) galaxies. Given the known distance of the MCs and low foreground Galactic absorption in their direction, outbursts of MC pulsars (e.g., see SMC X-2, SMC X-3, LXP 8.04; La Palombara et al. 2016; Tsygankov et al. 2017; Koliopanos & Vasilopoulos 2018; Vasilopoulos et al. 2014) can offer unique insight into super-critical accretion; i.e. the critical L_X where the shock is created above the NS and the accretion column is formed.

RX J0209.6−7427 is a BeXRB system discovered by analysis of archival ROSAT PSPC observations (Kahabka & Hilker 2005), and located in the outer wing of the Small Magellanic Cloud (SMC). The only two historic outbursts occurred in March and November 1993 and were detected by ROSAT PSPC (Kahabka & Hilker 2005). Both outbursts reached a luminosity of ~10^{38} erg s^{-1} (0.1–2.4 keV band) and lasted approximately one month, while the outburst peaks were separated by about 200 days. In 2019, RX J0209.6−7427 exhibited a major outburst where the X-ray luminosity of the system exceeded 10^{39} erg s^{-1}, thus the system temporarily became a PULX. Given the proximity of the system, and the accurately measured distance of the SMC, this offers an ideal opportunity to study its properties and compare them with PULXs and other HMXB pulsars that have exhibited super-Eddington outbursts.

In this paper we present the first results of the X-ray monitoring of the system during its 2019 outburst (see Section §2). In Section §3 we present the timing and spectral analysis that resulted in the discovery of coherent pulsations and characterization of its broadband X-ray spectrum from *NuSTAR* and *NICER* data. Finally from monitoring *Fermi*/GBM and *NICER* data obtained within the first 20 days of the outburst we can put strong constraints on the NS magnetic field strength (see §4).

2 THE 2019 OUTBURST OF RX J0209.6-7427

On 2019 November 20, the MAXI/GSC nova alert system triggered on an uncatalogued X-ray transient source (Negoro et al. 2019). Follow-up observations with the *Neil Gehrels Swift Observatory* were performed on 2019 November 21, providing a localization of the system (Kennea et al. 2019) at $\alpha_{\rm J2000}$ = 02$^{\rm h}$09$^{\rm m}$33$^{\rm s}$85 and $\delta_{\rm J2000}$ = −74°27′12″5, with a 2.8″ positional uncertainty. This position lies 2.9″ from the known HMXB RX J0209.6−7427. On 2019 November 21, *NICER* began observations of this target that continue till the submission of this paper (Iwakiri et al. 2019). During the same period the outburst was detected by *Fermi*/GBM, while

NuSTAR made a single Directors Discretionary Time (DDT) observation.

2.1 Data analysis

Below we provide basic information for the tools and methodology used for data extraction and analysis of the X-ray data obtained with *NuSTAR*, *NICER* and *Fermi*/GBM during the 2019 outburst of RX J0209.6−7427.

2.1.1 *NuSTAR*

The Nuclear Spectroscopic Telescope Array (*NuSTAR*) mission is the first focusing high-energy X-ray telescope in orbit operating in the band from 3 to 79 keV (Harrison et al. 2013). *NuSTAR* observed the system on 2019 November 26 with a 22 ks DDT observation (obsid: 90502352002, MJD start:58813.33760417). *NuSTAR* data were analysed with version 1.8.0 of the *NuSTAR* data analysis software (DAS), and instrumental calibration files from `CalDB` v20191008. The data were calibrated using the standard settings on the `NUPIPELINE` script, reducing internal high-energy background, and screening for passages through the South Atlantic Anomaly (see similar procedure in Koliopanos et al. 2019). Using the `NUPRODUCTS` script we extracted phase-averaged spectra for source and background regions (60″ radius), as well as instrumental responses for each of the two focal plane modules (FPMA/B). Finally, for timing studies we performed barycentric corrections to event time of arrivals.

2.1.2 *NICER*

The *NICER* X-ray Timing Instrument (XTI, Gendreau et al. 2012, 2016) is a non-imaging, soft X-ray telescope aboard the *International Space Station*. The XTI consists of an array of 56 co-aligned concentrator optics, each associated with a silicon drift detector (Prigozhin et al. 2012), operating in the 0.2–12 keV band. The XTI provides high time resolution ($\sim$ 100 ns) and spectral resolution of $\sim$ 85 eV at 1 keV. It has a field of view of $\sim$ 30 arcmin^2 in the sky and effective area of $\sim$1900 cm^2 at 1.5 keV (with the 52 currently active detectors).

For the current study we analysed *NICER* data obtained between MJD 58808–58834. Data were reduced using `HEASOFT` version 6.26.1, *NICER* DAS version 2019-06-19_V006a, and the calibration database (CALDB) version 20190516. For the timing analysis, we selected good time intervals according to the following conditions: *ISS* not in the South Atlantic Anomaly region, source elevation $>$ 20° above the Earth limb ($>$ 30° above the bright Earth), pointing offset $\leq$ 54 arcsec, and magnetic cutoff rigidity (`COR_SAX`) $>$ 1.5 GeV/c. For timing analysis, we performed barycentric corrections to event time of arrivals using the `barycorr` tool and the JPL DE405 planetary ephemeris.

For spectroscopy, we extracted spectra obtained quasi-simultaneously with *NuSTAR* (i.e., MJD 58813.382–58813.707, total exposure 865 s), in order to perform a broadband spectral fit. We generated the background spectrum from a grid of *NICER* blank-sky spectra corresponding to the blank-sky pointings of Rossi X-ray Timing Explorer (see Jahoda et al. 2006). This grid of spectra is populated with observed spectra in various space-weather observing conditions (K. C. Gendreau et al., in preparation). The background spectrum is generated by combining these blank-sky spectra weighted according to space-weather conditions and magnetic
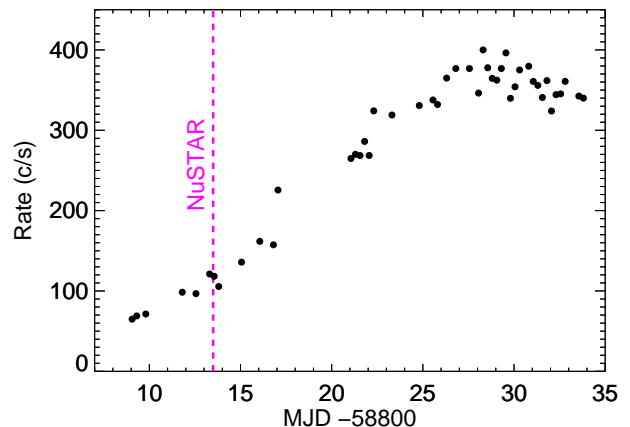
Figure 1. X-ray lightcurve of RX J0209.6−7427 based on *NICER* count rates (0.5-8.0 keV) averaged over 6 hour intervals. The dashed vertical line indicates the epoch of the *NuSTAR* observation. First *NICER* visit was performed within 1 day from the initial MAXI detection (Negoro et al. 2019). To translate *NICER* count rates to bolometric L_X we find a conversion factor of $\sim 4.75 \times 10^{36}$(erg/s)/(c/s) based on spectral fitting of the simultaneous obtained X-ray spectra (see § 3.1 for details).

cutoff rigidities common to both the pulsar and background-fields observations. For spectral fitting we used the latest available redistribution matrix and ancillary response files (v1.02).

2.1.3 *Fermi* GBM

The Gamma-ray Burst Monitor (GBM) on board *Fermi* (Meegan et al. 2009) is an all sky monitor consisting of 12 sodium iodide (NaI) detectors and two bismuth germanate (BGO) detectors. The NaI detectors are sensitive to hard X-rays from 8–1000 keV while the BGOs extend this energy to 40 MeV and are not sensitive to typical accreting binaries. There are three public data types available: CTIME which has 0.256 second timing resolution and 8 energy channels and is typically used for localization, transient detection, and this pulsar work, CSPEC which has 8 second timing resolution and 128 energy channels and is typically used for spectroscopy, and CTTE which is time tagged event data in 128 energy channels with 2 μs timing accuracy.

3 RESULTS

In Figure 1 we plot the X-ray lightcurve of RX J0209.6−7427 during its 2019 outburst as obtained by *NICER*. Given the brightness of the outburst no background subtraction was performed for the created lighcurve as its contribution is minimal ($<$ 1%). The outburst reached a peak flux in the *NICER* band around 20 days after its initial detection. For the current work we focus on the system's properties during a $\sim$25 day period after its original detection, which covers the rise of the outburst and is sufficient for our scientific goals. Further analysis of the data collected during the complete outburst will be presented in future publications.

3.1 Spectral properties

The X-ray spectra of BeXRBs show a power-law like shape having an exponential high energy cutoff (e.g., XSPEC models 'cutoffpl', 'highecut', 'bknpow', 'fdcut') that originates from the ac-
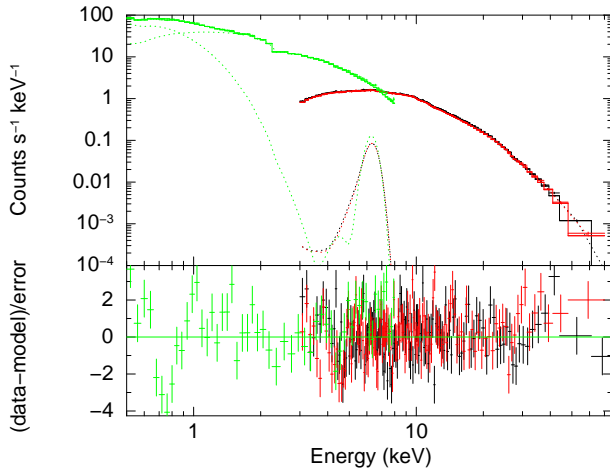
Figure 2. Phase averaged spectrum of RX J0209.6−7427 (upper panel) during the *NICER/NuSTAR* simultaneous observation. *NICER* (green points) and *NuSTAR* (black and red points for FPM A and B) data are plotted together with the best fit model (see Table 1). The individual spectral components (i.e. `diskbb`, `fdcut` and Gaussian line at 6.4 keV) are ploted with dashed lines .The lower panel shows the residuals to the best fit model. Events were re-binned for plotting purposes only.

Table 1. Best-fit parameters of the empirical model

	Parameter	Value	Units
	xspec model: Tbabs*(diskbb + fdcut + gaussian)		
	$N_{\rm H}$ Gal[a]	1.58 (fixed)	$10^{21}\,{\rm cm}^{-2}$
`diskbb`	$kT_{\rm BB}$	$0.192^{+0.007}_{-0.005}$	keV
	$Norm_{\rm BB}$ [b]	5100^{+700}_{-800}	$(R_{\rm BB}/D_{10})^2 \cos\theta$
	$R_{\rm BB}$ [b]	470^{+30}_{-40}	km
`fdcut`	Γ	0.802 ± 0.013	-
	E_c	$10.9^{+0.9}_{-0.8}$	keV
	E_f	$10.21^{+0.16}_{-0.14}$	keV
	Norm	$4.40^{+0.06}_{-0.08}$	$\times 10^{-2}$
`Gaussian`	$E_{\rm Fe}$	$6.34^{+0.06}_{-0.08}$	keV
	$\sigma_{\rm Fe}$ (keV)	$0.33^{+0.11}_{-0.06}$	keV
	Norm	$3.4^{+0.8}_{-0.4}$	$(10^{-4}\,{\rm cm}^{-2}\,{\rm s}^{-1})$
Other information			
	$C_{\rm FPMB}$ [c]	$1.039^{+0.003}_{-0.004}$	-
	$C_{\rm NICER}$ [c]	$0.989^{+0.011}_{-0.010}$	-
	red. χ^2/dof	1.06906/2332	
	$L_{\rm X}$ [d]	5.54 ± 0.05	10^{38} erg s^{-1}
	$\dot{M}(L_{\rm X})$ [e]	3.07 ± 0.03	10^{18} g s^{-1}

[a] Galactic absorption was fixed to this value (see text for details). [b] Disk radius was estimated from the normalization of the model, while assuming a disk inclination of 45° and distance of 55 kpc (i.e. $D_{10} = 5.5$). [c] The data from the 3 detectors were fitted simultaneously with all parameters tied apart from a constant that was left free to account for instrumental differences. [b] Unabsorbed X-ray luminosity in the (0.5–70 keV) band for a distance of 55 kpc. [d] Mass accretion rate onto the NS, assuming $L_{\rm X} = 0.2\dot{M}c^2$.

cretion column (e.g., Tsygankov et al. 2017; Maitra et al. 2018). In many cases BeXRB spectra show residuals at soft energies. These residuals are often referred to as a "soft-excess" whose physical origin is attributed to a combination of mechanisms like, emission from the accretion disk, emission from the NS surface, or hot plasma around the magnetosphere (Hickox et al. 2004). Due to the low foreground absorption, this "soft-excess" is often apparent in BeXRBs in the MCs (Bartlett et al. 2013; Sturm et al. 2014; Vasilopoulos et al. 2013, 2016).

We investigated the broadband spectrum of RX J0209.6−7427 using simultaneous *NICER* and *NuSTAR* data. Our goal is to fit the spectra using a phenomenological model and to measure the broadband (i.e., 0.5–70.0 keV) X-ray luminosity of the system. For spectral analysis all counts were regrouped to have at least 25 counts per bin. Spectral analysis was performed using XSPEC v12.10.1f (Arnaud 1996). Motivated by the spectral properties of BeXRBs, the *NICER* and *NuSTAR* spectra were fitted simultaneously with a standard phenomenological continuum composed of a soft black body and a power-law with high energy cut-off. To account for the photoelectric absorption by the interstellar gas we used `tbabs` in `xspec` with Solar abundances set according to Wilms et al. (2000) and atomic cross sections from Verner et al. (1996). Column density was fixed[1] to the Galactic value of 1.58×10^{21} cm^{-2} (Dickey & Lockman 1990).

Among the tested power-law models, the best fit was obtained by 'fdcut' (Tanaka 1986). This model is a smoothed power-law

---

[1] We also tested a combination of two absorption components to account for Galactic absorption and intrinsic absorption as it is typical for BeXRBs in the Magellanic Clouds (e.g. Vasilopoulos et al. 2013, 2016, 2017, 2018a). The second component was left free to account for the absorption near the source or within the SMC, thus elemental abundances were fixed at 0.2 solar (Russell & Dopita 1992). However, the second component was not constrained by the fit and its column density was consistent zero, thus was not used in the reported spectral fit.

with cut-off and is expressed analytically as:

$$dN/dE = E^{-\Gamma}\left(1 + \exp\frac{E - E_c}{E_f}\right)^{-1}. \qquad (1)$$

We note that non-smoothed models like 'highecut' created sharp residuals around the cut-off energy that could be confused with absorption lines related to cyclotron scattering features that are often found in this energy range. A soft spectral component is needed to obtain an acceptable fit, we decided to use a typical disc black body (`diskbb` in `xspec`). In the residuals of the fitted model there is clear evidence of an emission line present at ∼ 6.4 keV that originates from neutral Fe (Kα line). The width of the Gaussian line (∼ 0.3 keV) is comparable to that of other BeXRBs during major outbursts (e.g., Swift J0243.6+6124; Jaisawal et al. 2019). In regards to the best fitted model, there are still residuals around 1 keV that could be related to a mixture of emission lines as seen in other BeXRBs (e.g., see SMC X-3, Koliopanos & Vasilopoulos 2018). Investigating the nature of these residuals is beyond the scope of the paper[2]. To estimate uncertainties we used Markov Chain Monte Carlo sampling method (available through `xspec`). We used the Goodman-Weare algorithm to create a chain (total

---

[2] Due to limited calibration of *NICER* around 1 keV it is quite possible that the origin of these features is a mixture of physical and instrumental effects.
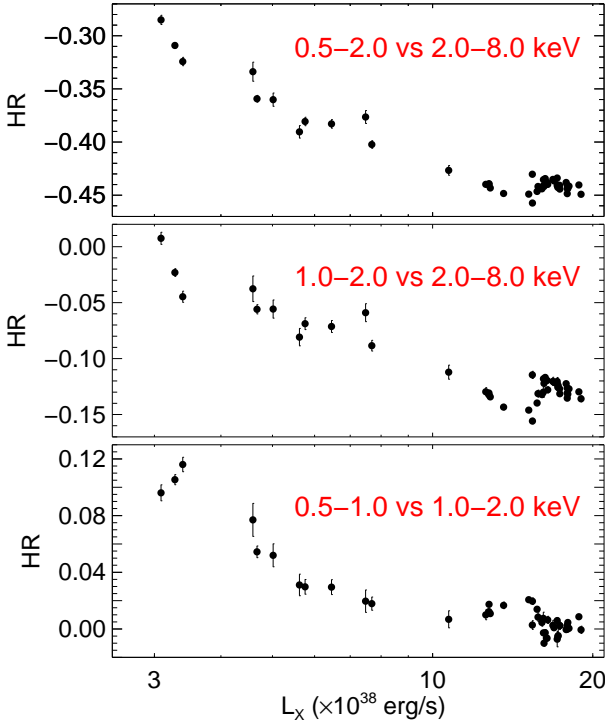
Figure 3. Spectral hardness of RX J0209.6−7427 as a function of X-ray luminosity. From top to bottom HRs are computed from *NICER* data using different detector energy bands. For each point we summed events collected within a maximum of a 6 hours period.

Table 2. Pulse Timing Parameters for RX J0209.6−7427

Fit and data-set	
MJD range	58808.9—58835.5
Number of TOAs	85
Rms timing residual (ms)	36
Set Quantities	
Right ascension, α (hh:mm:ss)	02:09:34.76
Declination, δ (dd:mm:ss)	−74:27:14.0
Epoch of frequency determination t_0 (MJD) .	58822
Measured Quantities	
Pulse frequency, ν_0 (s^{-1})	0.1075687(2)
First derivative of pulse frequency, $\dot{\nu}$ (s^{-2}) . . .	1.165(3)×10^{-10}
Second derivative of pulse frequency, $\ddot{\nu}$ (s^{-3})	1.26(2)×10^{-16}
Whitening terms	
Reference epoch for Waves	58822
Fundamental Wave frequency, ω_{pw} (rad yr^{-1})	48.0217
Wave 1: $A_{cos,1}$; $A_{sin,1}$	24.6002; −25.2251
Wave 2: $A_{cos,2}$; $A_{sin,2}$	-21.6411; 42.6438
Wave 3: $A_{cos,3}$; $A_{sin,3}$	19.1398; −28.4544
Wave 4: $A_{cos,4}$; $A_{sin,4}$	−4.15159; 11.3984
Wave 5: $A_{cos,5}$; $A_{sin,5}$	0.183705; −1.80281
Assumptions	
Solar system ephemeris model	DE405
Time units	TDB

length of 10,000) of parameter values and create a probability distribution for each free parameter. The best fit parameters (with their 90% uncertainties) are presented in Table 1 and the spectrum is shown in Figure 2. From the best fit model we are able to derive a conversion factor (i.e., C_{bol}) to translate *NICER* count rates (0.5–8.0 keV band) to "bolometric" X-ray luminosity (i.e., 0.5–70.0 keV) band. Assuming a distance[3] to the source of 55 kpc (Harries et al. 2003), we estimated $C_{bol} \approx 4.75 \times 10^{36}$ (erg/s)/(c/s).

To track the spectral evolution of RX J0209.6−7427 during its 2019 outburst, we used the hardness ratio (HR), defined as HR = $(R_{i+1} − R_i)/(R_{i+1} + R_i)$, where R_i is the count rate in a specific energy band. We split the collected events in 6 h intervals and computed HR using the 0.5–2.0 keV and 2.0–8.0 keV energy bands. We further computed HR indices using different *NICER* energy bands. In the hard bands (1.0-2.0 vs 2.0-8.0 keV), HR is representative of changes of the power-law continuum. While in the soft bands (0.5-1.0 vs 1.0-2.0 keV), HR evolution is representative of the soft-excess and possible changes in absorption. We found no visual evidence of rapid changes in HR evolution that could be related with rapid increase in absorption (i.e. sudden increase in soft HR). In Figure 3 we plot HR as a function of the broadband L_X computed by translating *NICER* count rates to L_X using C_{bol} (see similar application to SMC X-3; Tsygankov et al. 2017). Given that there is a spectral change with L_X, this linear conversion from count rates to L_X should have an uncertainty of a factor of 30-50%. Given that

the spectrum becomes softer-when-brighter, around the peak of the outburst L_X should be overestimated by a small factor.

3.2 Temporal properties

In all *NICER* observations, a periodic modulation is apparent even by eye if we appropriately re-bin the events. A pulsation search using PRESTO (Ransom et al. 2002) on the barycentered event data confirmed the coherent pulsations with a period of 9.29 s (reported by Iwakiri et al. 2019). Pulsations near this period are detected in all *NICER* observations as well as in the *NuSTAR* TOO observation. Following the period-based nomenclature introduced by Coe et al. (2005) for BeXRB pulsars in the SMC, an alternative designation for RX J0209.6−7427 is SXP 9.3.

The pulse period has been decreasing during the outburst. We generated a phase-coherent timing model for all the data analysed here (i.e. ~25 days) using Tempo2 (Hobbs et al. 2006). To do this, we subdivided the data into intervals of less than 3000 seconds and generated one TOA per interval by cross-correlating a folded pulse profile with an analytic template composed of 4 gaussians (Ray et al. 2011). We fitted the TOAs to a timing model with two frequency derivatives, i.e. $\nu(t) = \nu_0 + \dot{\nu}(t − t_0) + (1/2)\ddot{\nu}(t − t_0)^2$ while setting t_0 to 58810 MJD. Nevertheless, there are substantial systematic residuals likely caused by torque noise. We added a set of harmonically-related sinusoids (WAVE parameters in Tempo2) to obtain a model with nearly white residuals. The results of the coherent timing analysis are summarized in Table 2.

A search for pulsations was performed in the direction of RX J0209.6−7427 in GBM data around the *NICER* frequency in the manner described in Finger et al. (1999) and Jenke et al. (2012). Specifically we used CTIME data products. Pulsation search was initially performed over 1000 frequencies from 106.91732 mHz to 108.07473 mHz as well as the next two harmonics in the energy range between 12.0-50.0 keV, over two day intervals. Once a phase model was established for the spin-up of the pulsar, the frequency search was repeated over the centroid frequency from the phase model plus and minus 50 increments of 925.9259×10^{-5}
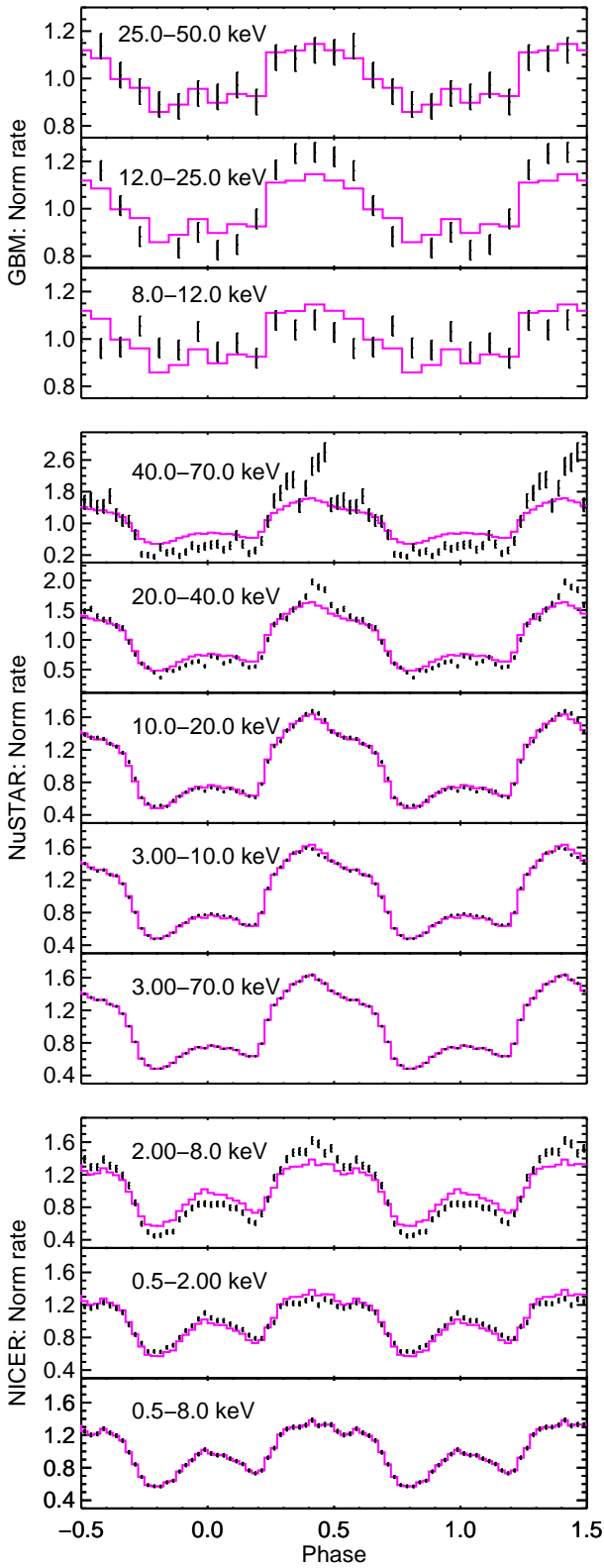
---

[3] Although the distance to the SMC is found to be ~ 62 kpc (Graczyk et al. 2014), for BeXRBs located at the SMC wing (e.g. Hénault-Brunet et al. 2012), a distance of 55 kpc is commonly adopted (Cignoni et al. 2009).

Figure 4. Energy resolved pulse profiles for RX J0209.6−7427 obtained by quasi-simultaneous observations (see text). Each panel contains points from the corresponding energy band (see legend), while with magenta lines we plot the average pulse profile for each instrument.
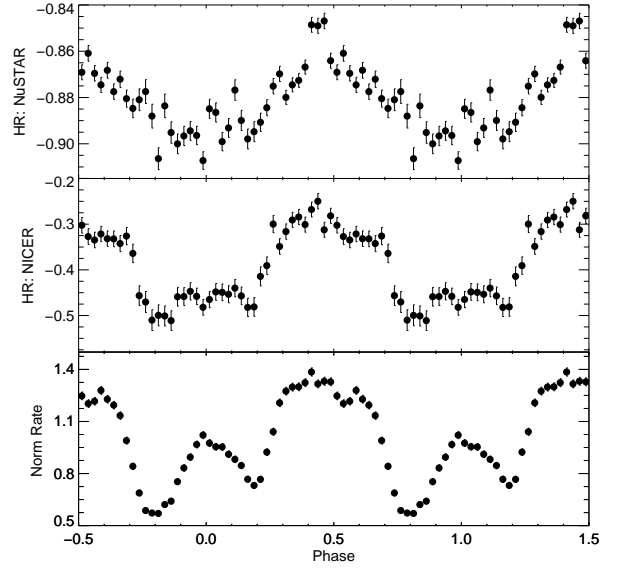

Figure 5. Pulse phase resolved hardness ratios of RX J0209.6−7427 obtained by quasi-simultaneous observations (see text). For the *NuSTAR* HR (upper panel) we have used the 3.0–20.0 keV and 20.0–70.0 keV energy bands. For the *NICER* HR (middle panel) we have used the 0.5–2.0 keV and 2.0–8.0 keV energy bands. In the lower panel we have plotted the average (0.5–8.0 keV) pulse profile obtained by *NICER*.
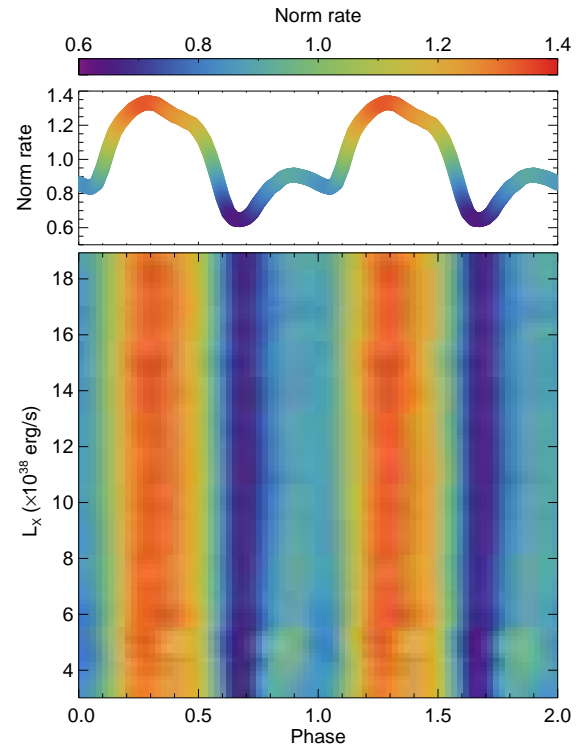

Figure 6. *Lower panel:* Heat map of the pulse profile evolution as a function of pulse-averaged L_X (0.5–70 keV) for the 25 first days of the outburst. The normalization is based on the L_X derived from the broadband spectral fit. *Upper panel:* For comparison we have plotted the averaged pulse profile from the same period.

mHz. A search over 160 frequency derivatives was also added. These where centered on the phase model frequency derivative at even intervals of 3.282×10^{-12} cycles/s/s. The fitted Fourier amplitudes for the six harmonics with the frequency and frequency derivative that resulted in the maximum Y_n statistic, as described in Finger et al. (1999), and a Y_n statistic that exceeded 35 were retained. The lowest Y_n statistic was 59 for the first interval while the remainder of the detected frequencies had a Y_n statistic exceeding 100 signifying a reliable detection. A search with one day integrations was also performed and resulted in a poorer determination of the frequency derivative. The results are publicly available through the *Fermi*/GBM accreting pulsars project[4]. To compare the temporal properties of RX J0209.6−7427 obtained by *Fermi*/GBM with those obtained by *NICER* and *NuSTAR* we used GBM data within a one day period following MJD 58813-14.

To investigate changes of the pulse profile with energy we analysed all data obtained quasi-simultaneously with *NuSTAR* (see §2.1). In Figure 4 we present the pulse profiles for individual instrument bands, while in Figure 5 we present the pulse phase resolved hardness ratios for *NICER* and *NuSTAR*. Both *NuSTAR* and *NICER* events were folded based on the same ephemeris. The pulse profile is double peaked at low energies while it gradually changes to single peaked at high energies.

In order to visualize the pulse profile evolution we created a heat map of the pulse shape as a function of pulse averaged L_X. For this purpose we used only *NICER* data. We split the events into 1 day intervals, assigned phases using the model in Table 2 and created pulse profiles using 40 phase bins. Each profile was smoothed and normalized with its average count rate. We then created a 2D histogram of the intensity of the system in pulse-phase and average pulse intensity. Finally, we converted *NICER* count rates to broadband L_X by using the conversion factor obtained by the broadband spectral fit. The resulting heat-map is shown in Figure 6. The pulse-profile showed minimal evolution with L_X, maintaining its double peaked shape. The only evident change was that the "trough" between the two main peaks (i.e. phase 1.0–1.1 in Fig. 6) became shallower at large L_X. The feature at 5×10^{38} erg s^{-1} is due to lower statistics during that period.

3.3 NS magnetic field from spin-up

Changes in the spin of a NS due to accretion can be predicted by theoretical models, if at least two parameters are known; the accretion rate (i.e., $\dot{M}$) and the surface magnetic field (i.e., B) of the NS (Wang 1995). Mass is transferred from the inner radius of a Keplerian disc that is truncated at the magnetospheric radius due to the balance of magnetic and gas pressures (Ghosh et al. 1977):

$$R_M = \xi \left(\frac{R_{NS}^{12} B^4}{2 G M_{NS} \dot{M}^2} \right)^{1/7}, \qquad (2)$$

where G is the gravitational constant, M_{NS} and R_{NS} is the NS mass and radius and $\xi \sim 0.5$ (Campana et al. 2018) is a scaling factor between magnetospheric radius (R_M) and Alfvál'n radius for disc accretion.

As material is deposited onto the magnetic pole of the NS (see Becker & Wolff 2007), the bolometric X-ray luminosity emitted can be converted to a mass accretion rate $\dot{M}$ assuming some efficiency η_{eff} (i.e., $L_X \approx \eta_{eff} \dot{M} c^2$). This is generally assumed to
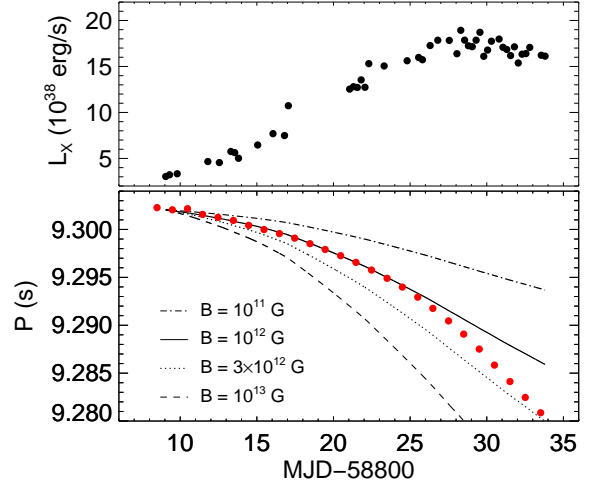
Figure 7. *Upper panel:* X-ray light-curve of SXP 9.3 (0.5-70 keV), where L_X is estimated by scaling the *NICER* count rates with the correction factor estimated by the simultaneous *NICER* and *NuSTAR* spectral fit. *Lower panel:* Spin period measurements based on *Fermi*/GBM data (red points). With various lines we mark the predicted evolution of P for different values of the NS magnetic field (see text for details).

be the efficiency under which gravitational energy is converted to radiation, namely $L_X = G M_{NS} \dot{M}/R$. For $R = R_{NS} = 10^6$ cm and $M_{NS} = 1.4 M_\odot$, one finds $L_X \approx 0.2 \dot{M} c^2$ (Henceforth, we adopt $\eta_{eff} = 0.2$).

The induced torque due to the mass accretion is $N_{acc} \approx \dot{M} \sqrt{G M_{NS} R_M}$. The total torque can be expressed in the form of $N_{tot} = n(\omega_{fast}) N_{acc}$ where $n(\omega_{fast})$ is a dimensionless function that accounts for the coupling of the magnetic field lines to the accretion disc and takes the value $\approx 7/6$ for slow rotators (for more details see Wang 1995; Parfrey et al. 2016). The spin-up rate of the NS is then given by:

$$\dot{\nu} = \frac{n(\omega_{fast})}{2\pi I_{NS}} \dot{M} \sqrt{G M_{NS} R_M}, \qquad (3)$$

where $I_{NS} \simeq (1 - 1.7) \times 10^{45}$ g cm^2 is the moment of inertia of the NS (e.g., Steiner et al. 2015). Henceforth, we adopt $I_{NS} \simeq 1.3 \times 10^{45}$ g cm^2.

The spin period (or frequency) evolution of the NS can then be derived by solving Equation 3 for a variable $\dot{M}(t)$ and a constant B value. The details of the methodology we followed are presented in the study of the spin-period evolution of NGC 300 ULX-1 (Vasilopoulos et al. 2019). In the case of RX J0209.6−7427 the evolution of $\dot{M}$ during the outburst can be derived from the observed *NICER* light curve assuming the scaling factor (count rate to L_X) derived from the broadband spectral fit (see §3.1), and for various values of B. The derived spin-period evolutionary tracks are plotted together with the observed values in Figure 7. From the figure it is clear that the observed evolution of P is consistent with $B = 1{-}3 \times 10^{12}$ G. Given the fact that we used a linear conversion from *NICER* count rates to $\dot{M}$ our estimation should have a systematic uncertainty and thus B could be underestimated by a factor of 2. Moreover, it seems that the observed evolution of P does not show any visual signature related to orbital Doppler shifts. As we will discuss in the next paragraph, although we cannot measure the orbital parameters, we can put constraints on the orbital period and perhaps inclination of the binary plane.

3.4 Constraints on binary orbital parameters from spin-up

As of December 16 2019, the spin frequency of the NS in RX J0209.6−7427 is increasing continually, while its evolution is consistent with spin-up due to accretion. Specifically between MJD 58810-58826 the spin evolution of the NS is consistent with the predictions of spin-up due to accretion, while between MJD 58826-58835 we see a deviation that is probably associated with orbital Doppler shifts. Although an orbital signal is not yet evident in the data we can perform an exercise to demonstrate the effect of a fiducial binary orbit on the observed period of the NS. We simulated circular binary orbits and estimated the radial velocity of the NS, and thus the change in the observed period due to Doppler shifts. The mass of the NS was kept constant to $1.4 M_\odot$, while other parameters were assigned from uniform distributions; i.e., the mass of the donor star ($M_{star} \in [8, 10] \ M_\odot$), the orbital period ($P_{orb} \in [10, 250] \ d$) and the binary plane inclination in respect to the observer ($\theta \in [0, 90]^o$). In Figure 8 we plot the observed periods from *Fermi*/GBM together with predictions of random orbital models.

4 DISCUSSION

We studied properties of the SMC BeXRB RX J0209.6−7427 based on X-ray data collected during a ~25 day period of its 2019 giant outburst. Analysis of the *NICER* and *Fermi*/GBM data yielded the discovery of its spin period (~ 9.3 s). The pulse profile of the NS is double peaked at low energies while its pulsed fraction increases at higher energies (see Figure 4). During the evolution of the outburst there was minimal change in its pulse profile at low energies (see Figure 6). Broadband spectroscopy performed on *NICER* and *NuSTAR* data enabled us to approximate its spectrum with a phenomenological model which provided a good estimate of a correction factor to transform *NICER* count rates (0.5–8 keV) to broadband L_X (0.5–70 keV). We used *Fermi*/GBM data to follow the spin evolution of the NS and compare it with the theoretically predicted spin-up due to accretion. We thus concluded that the surface magnetic field of the NS should be ~1–3×10¹² G, while its orbital period is most probably larger than 50 days.

The spectral shape of accreting X-ray pulsars depends on the accretion regime. The dependence of the spectral hardness with L_X has been shown to follow two different regimes (e.g., Reig & Nespoli 2013). In the subcritical regime the spectrum of the pulsar becomes harder when brighter, while in the supercritical regime the opposite behavior takes place. For the pulsars studied by Reig & Nespoli (2013), the critical L_X where the turn from subcritical to supercritical regime occurs around $1 − 2 \times 10^{37}$ erg s⁻¹ (0.3–10.0 keV band). The transition should be related to a formation of a shock above the NS hot spot, where material is deposited (Becker & Wolff 2007). While for different BeXRBs, this transition should provide hints for the magnetic field strength of the NS, as the cross-section for the scattering of in-falling material is a function of B (Canuto et al. 1971; Lodenquai et al. 1974). However, it should be noted that the softer-when-brighter dependence only refers to the phase-average properties. The opposite behaviour occurs within the pulse phase, where the spectrum becomes harder with increased pulsed intensity (see Figure 5). This is quite typical to X-ray pulsars and is related to the anisotropic emission from the accretion column. In fact the double peaked pulse profile of RX J0209.6−7427 is characteristic of BeXRBs in the supercritical regime, as is typically considered a signature of radiation escaping from the sides of the accretion column in a fan-beam emission pattern (Basko & Sunyaev 1975).

In Figure 3 we show the spectral hardness as a function of L_X. The source behavior at $L_X = (2−10) \times 10^{38}$ erg s⁻¹ is consistent with the supercritical regime, i.e., the diagonal branch of the hardness-intensity diagrams (Reig & Nespoli 2013). In addition, the figure indicates the presence of perhaps a third branch that appears above 10^{39} erg s⁻¹, which is similar to the spectral evolution of SMC X-3 during its 2016 outburst (Koliopanos & Vasilopoulos 2018). In that case, Koliopanos & Vasilopoulos (2018) claimed that this stabilization might have eluded detection because the sources studied by Reig & Nespoli (2013) never reached such high L_X. It is plausible that the spectral hardness stabilization is a manifestation of physical changes in the accretion column; i.e, the accretion column reached its maximum height and/or the optical depth of the in-flowing material exceeded unity. Moreover, the HR does not have the necessary sensitivity to trace complicated changes in the spectral shape. For example, the "soft-excess" typically becomes brighter with L_X thus resulting in softer HR, a stabilization of the HR could be a result of the "soft-excess" reaching a saturation limit (see SMC X-3 case, Koliopanos & Vasilopoulos 2018). In addition the high energy cutoff of the spectrum typically moves to lower energies as the source optical depth in the accretion column becomes higher. A detailed study of these effects is beyond the scope of this paper.

The spectral (i.e., softer-when-brighter evolution) and temporal (i.e., double peaked pulse profile and spin-evolution) properties of RX J0209.6−7427 are evidence of the system remaining in the super-critical regime during the observed period. At this point we can estimate the critical L_{crit} where the accretion column is formed resulting in a pivot point in the spectral hardness evolution with L_X. Following Becker et al. (2012) this is given by:

$$L_{crit} = \left(\frac{B}{0.688 \times 10^{12} \ G} \right)^{16/15} \times 10^{37} \ \text{erg/s}, \quad (4)$$

that holds for typical parameters for the NS mass ($M_{NS} = 1.4 M_\odot$), radius ($R_{NS} = 10$ km), standard disk accretion, and an accretion column where the seed photons inside the column originate from bremsstrahlung emission (see eq. 32 of Becker et al. 2012, for more details). For $B = 1 − 3 \times 10^{12}$ G, equation 4 yields a critical $L_{crit} \sim 1.5 − 4.4 \times 10^{37}$ erg s⁻¹. Monitoring observations during the decay of the outburst could verify our estimated B value through more detailed timing analysis (i.e., if an orbital modulation is found), or spectral transition in the context of Reig & Nespoli (2013).

Another mechanism that is often used to probe the dipole B strength of the NS in BeXRBs is the propeller transition (Illarionov & Sunyaev 1975). Although, the transition between accretor regimes and propeller is often missed due to observational sampling (e.g., Vasilopoulos et al. 2017), we generally expect to observe a sharp drop in the observed flux when this occurs (e.g., Corbet 1996; Cui 1997; Tsygankov et al. 2016). Assuming $B = 1 − 3 \times 10^{12}$ G for RX J0209.6−7427 we found a limiting luminosity ($L_{X,Lim}$) of $1 − 9 \times 10^{35}$ erg s⁻¹ before the onset of propeller transition (see eq. 3 of Campana et al. 2018). For comparison for $B = 10^{13}$ G we would expect $L_{X,Lim} \sim 10^{37}$ erg s⁻¹ (i.e., $L_X \propto B^2$).

In the context of PULXs, RX J0209.6−7427 is yet another example of a system that can reach super-Eddington luminosity even though the NS has a typical B field strength, which is in agreement with the properties of the majority of known PULXs (King & Lasota 2019). Moreover, there is no change in the pulse profile of the system with L_X, thus there is no evidence of beaming of the pulsed component as the BeXRB luminosity exceeds super-Eddington limit.
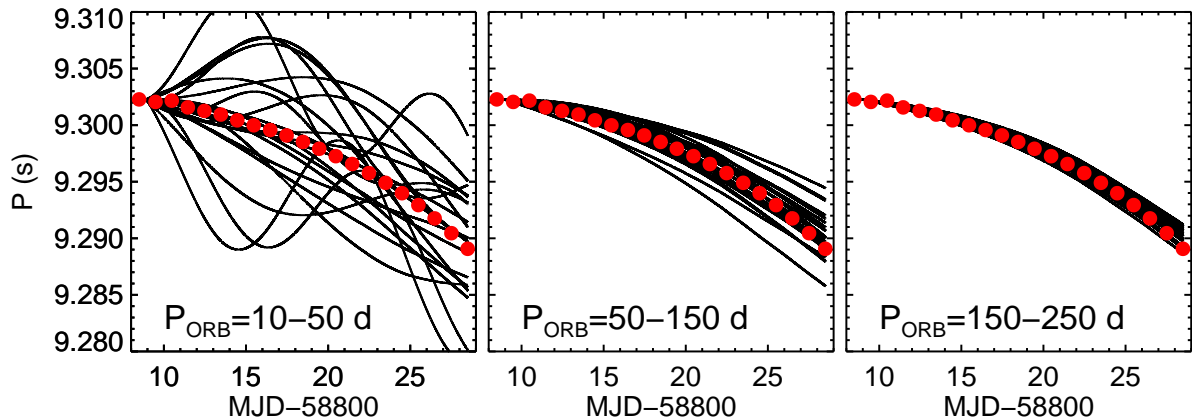
Figure 8. Fiducial evolution of observed period based on random orbital periods and inclination of the orbital plane in respect to the observer (see text). Similar to Figure 7, we calculated the accretion torques based on observed L_X and $B = 2 \times 10^{12}$ G. The lack of any apparent orbital signature in the data indicate that the orbital period of the system should be larger than ∼50 d, or that the binary system is observed face on.

5 CONCLUSION

RX J0209.6−7427 is a BeXRB system located in the outer SMC wing that exhibited a super-Eddington outburst in November 2019. The analysis of *NICER* data revealed the presence of coherent pulsations with a period of ∼ 9.3 s. During the outburst we obtained simultaneous *NICER* and *NuSTAR* observations that enabled us to perform broadband spectroscopy, thus characterizing its spectral shape and accurately measuring its X-ray luminosity. Moreover, no evidence of a cyclotron resonance feature was found in the *NuSTAR* spectrum of the source. From *NICER* monitoring data of the outburst we found that NS reached a peak luminosity of ∼ 2×10^{39} erg s^{-1} (0.5–70 keV), momentarily making RX J0209.6−7427 a ULX pulsar, and perhaps the brightest BeXRB ever observed in the SMC. Furthermore, we used *Fermi*/GBM data to follow the spin evolution of the NS and compare it with the theoretically predicted spin-up due to accretion. We thus concluded that the surface magnetic field of the NS is ∼3×10^{12} G and its orbital period is likely ≳50 days.

REFERENCES

Arnaud K. A., 1996, in Jacoby G. H., Barnes J., eds, Astronomical Society of the Pacific Conference Series Vol. 101, Astronomical Data Analysis Software and Systems V. p. 17
Bachetti M., et al., 2014, Nature, 514, 202
Bachetti M., et al., 2020, ApJ, 891, 44
Bartlett E. S., Coe M. J., Ho W. C. G., 2013, MNRAS, 436, 2054
Basko M. M., Sunyaev R. A., 1975, A&A, 42, 311
Basko M. M., Sunyaev R. A., 1976, MNRAS, 175, 395

Becker P. A., Wolff M. T., 2007, ApJ, 654, 435
Becker P. A., et al., 2012, A&A, 544, A123
Campana S., Stella L., Mereghetti S., de Martino D., 2018, A&A, 610, A46
Canuto V., Lodenquai J., Ruderman M., 1971, Phys. Rev. D, 3, 2303
Carpano S., Haberl F., Maitra C., Vasilopoulos G., 2018, MNRAS, 476, L45
Casares J., Negueruela I., Ribó M., Ribas I., Paredes J. M., Herrero A., Simón-Díaz S., 2014, Nature, 505, 378
Cignoni M., et al., 2009, AJ, 137, 3668
Coe M. J., Edge W. R. T., Galache J. L., McBride V. A., 2005, MNRAS, 356, 502
Corbet R. H. D., 1996, ApJ, 457, L31
Cui W., 1997, ApJ, 482, L163
Dauser T., Middleton M., Wilms J., 2017, MNRAS, 466, 2236
Dickey J. M., Lockman F. J., 1990, ARA&A, 28, 215
Epili P., Naik S., Jaisawal G. K., Gupta S., 2017, MNRAS, 472, 3455
Finger M. H., Bildsten L., Chakrabarty D., Prince T. A., Scott D. M., Wilson C. A., Wilson R. B., Zhang S. N., 1999, ApJ, 517, 449
Fürst F., et al., 2016, ApJ, 831, L14
Fürst F., Walton D. J., Stern D., Bachetti M., Barret D., Brightman M., Harrison F. A., Rana V., 2017, ApJ, 834, 77
Gendreau K. C., Arzoumanian Z., Okajima T., 2012, The Neutron star Interior Composition ExploreR (NICER): an Explorer mission of opportunity for soft x-ray timing spectroscopy. p. 844313, doi:10.1117/12.926396
Gendreau K. C., et al., 2016, The Neutron star Interior Composition Explorer (NICER): design and development. p. 99051H, doi:10.1117/12.2231304
Ghosh P., Lamb F. K., Pethick C. J., 1977, ApJ, 217, 578
Graczyk D., et al., 2014, ApJ, 780, 59
Haberl F., 1995, A&A, 296, 685
Harries T. J., Hilditch R. W., Howarth I. D., 2003, MNRAS, 339, 157
Harrison F. A., et al., 2013, ApJ, 770, 103
Hénault-Brunet V., et al., 2012, MNRAS, 420, L13
Hickox R. C., Narayan R., Kallman T. R., 2004, ApJ, 614, 881
Ho W. C. G., Klus H., Coe M. J., Andersson N., 2014, MNRAS, 437, 3664
Hobbs G. B., Edwards R. T., Manchester R. N., 2006, MNRAS, 369, 655
Illarionov A. F., Sunyaev R. A., 1975, A&A, 39, 185
Israel G. L., et al., 2017, Science, 355, 817
Iwakiri W., et al., 2019, The Astronomer's Telegram, 13309, 1
Jahoda K., Markwardt C. B., Radeva Y., Rots A. H., Stark M. J., Swank J. H., Strohmayer T. E., Zhang W., 2006, ApJS, 163, 401
Jaisawal G. K., et al., 2019, ApJ, 885, 18
Jenke P. A., Finger M. H., Wilson-Hodge C. A., Camero-Arranz A., 2012, ApJ, 759, 124
Kaaret P., Feng H., Roberts T. P., 2017, ARA&A, 55, 303
Kahabka P., Hilker M., 2005, A&A, 435, 9

Kennea J. A., et al., 2019, The Astronomer's Telegram, 13303, 1

King A., Lasota J.-P., 2019, MNRAS, 485, 3588

Koliopanos F., Vasilopoulos G., 2018, A&A, 614, A23

Koliopanos F., Vasilopoulos G., Godet O., Bachetti M., Webb N. A., Barret D., 2017, A&A, 608, A47

Koliopanos F., Vasilopoulos G., Buchner J., Maitra C., Haberl F., 2019, A&A, 621, A118

La Palombara N., Sidoli L., Pintore F., Esposito P., Mereghetti S., Tiengo A., 2016, MNRAS, 458, L74

Lodenquai J., Canuto V., Ruderman M., Tsuruta S., 1974, ApJ, 190, 141

Maitra C., Paul B., Haberl F., Vasilopoulos G., 2018, MNRAS, 480, L136

Martin R. G., Nixon C., Armitage P. J., Lubow S. H., Price D. J., 2014, ApJ, 790, L34

Meegan C., et al., 2009, ApJ, 702, 791

Middleton M. J., Fragile P. C., Ingram A., Roberts T. P., 2019, MNRAS, 489, 282

Mushtukov A. A., Suleimanov V. F., Tsygankov S. S., Poutanen J., 2015, MNRAS, 454, 2539

Negoro H., et al., 2019, The Astronomer's Telegram, 13300, 1

Okazaki A. T., Negueruela I., 2001, A&A, 377, 161

Okazaki A. T., Hayasaki K., Moritani Y., 2013, PASJ, 65, 41

Parfrey K., Spitkovsky A., Beloborodov A. M., 2016, ApJ, 822, 33

Pintore F., Zampieri L., Stella L., Wolter A., Mereghetti S., Israel G. L., 2017, ApJ, 836, 113

Prigozhin G., et al., 2012, Characterization of the silicon drift detector for NICER instrument. p. 845318, doi:10.1117/12.926667

Ransom S. M., Eikenberry S. S., Middleditch J., 2002, AJ, 124, 1788

Ray P. S., et al., 2011, ApJS, 194, 17

Ray P. S., et al., 2019, arXiv e-prints, p. arXiv:1903.03035

Reig P., 2011, Ap&SS, 332, 1

Reig P., Nespoli E., 2013, A&A, 551, A1

Rodríguez Castillo G. A., et al., 2019, arXiv e-prints, p. arXiv:1906.04791

Russell S. C., Dopita M. A., 1992, ApJ, 384, 508

Sathyaprakash R., et al., 2019, MNRAS, 488, L35

Steiner A. W., Gandolfi S., Fattoyev F. J., Newton W. G., 2015, Phys. Rev. C, 91, 015804

Sturm R., Haberl F., Pietsch W., Coe M. J., Mereghetti S., La Palombara N., Owen R. A., Udalski A., 2012, A&A, 537, A76

Sturm R., Haberl F., Vasilopoulos G., Bartlett E. S., Maggi P., Rau A., Greiner J., Udalski A., 2014, MNRAS, 444, 3571

Tanaka Y., 1986, Observations of Compact X-Ray Sources. p. 198, doi:10.1007/3-540-16764-1_12

Torrejón J. M., Orr A., 2001, A&A, 377, 148

Tsygankov S. S., Lutovinov A. A., Doroshenko V., Mushtukov A. A., Suleimanov V., Poutanen J., 2016, A&A, 593, A16

Tsygankov S. S., Doroshenko V., Lutovinov A. A., Mushtukov A. A., Poutanen J., 2017, A&A, 605, A39

Vasilopoulos G., Maggi P., Haberl F., Sturm R., Pietsch W., Bartlett E. S., Coe M. J., 2013, A&A, 558, A74

Vasilopoulos G., Haberl F., Sturm R., Maggi P., Udalski A., 2014, A&A, 567, A129

Vasilopoulos G., Haberl F., Delvaux C., Sturm R., Udalski A., 2016, MNRAS, 461, 1875

Vasilopoulos G., Haberl F., Maggi P., 2017, MNRAS, 470, 1971

Vasilopoulos G., Maitra C., Haberl F., Hatzidimitriou D., Petropoulou M., 2018a, MNRAS, 475, 220

Vasilopoulos G., Haberl F., Carpano S., Maitra C., 2018b, A&A, 620, L12

Vasilopoulos G., Petropoulou M., Koliopanos F., Ray P. S., Bailyn C. B., Haberl F., Gendreau K., 2019, MNRAS, 488, 5225

Vasilopoulos G., Lander S. K., Koliopanos F., Bailyn C. D., 2020, MNRAS, 491, 4949

Verner D. A., Ferland G. J., Korista K. T., Yakovlev D. G., 1996, ApJ, 465, 487

Walton D. J., et al., 2018a, ApJ, 856, 128

Walton D. J., et al., 2018b, ApJ, 857, L3

Wang Y.-M., 1995, ApJ, 449, L153

West B. F., Wolfram K. D., Becker P. A., 2017, ApJ, 835, 129

Wilms J., Allen A., McCray R., 2000, ApJ, 542, 914

Wilson-Hodge C. A., et al., 2018, ApJ, 863, 9

Zhang S., et al., 2019, Science China Physics, Mechanics, and Astronomy, 62, 29502

This paper has been typeset from a TeX/LaTeX file prepared by the author.